RSC Sustainability

ROYAL SOCIETY OF CHEMISTRY

COMMUNICATION

View Article Online
View Journal | View Issue

Cite this: *RSC Sustainability*, 2025, **3**, 3910

Received 29th April 2025
Accepted 14th July 2025

DOI: 10.1039/d5su00311c

rsc.li/rscsus

Immobilization of aldehyde reductase for the production of bioplastic precursors from agricultural fatty acids†

Devesh Mohne,[ab] Yeddula Nikhileshwar Reddy,[a] Kshitij Rawat,[ab] Mahesh D. Patil *[acd] and Jayeeta Bhaumik *[a]

Herein, we report the biosynthesis of bioplastic precursors thourgh the immobilization of aldehyde reductase (AHR) onto a metal organic framework (UIO-66-NH_2). Kinetic analysis demonstrated that the immobilized AHR maintained significant catalytic activity and exhibited improved operational stability, as well as higher reusability, compared with the free AHR. Furthermore, the synthetic applicability of the immobilized AHR was evaluated in tandem with that of transaminase derived from *S. pomeroyi* (spTA), where 8, 10, and 12 carbon chain ω-amino fatty acids (ω-AFAs) were biosynthesized from the corresponding hydroxy fatty acids (ω-HFAs) with ~90% conversions.

Sustainability spotlight

The annual global plastic production has crossed 400 million metric tons, significantly contributing to environmental pollution and the depletion of fossil resources. In response, this work offers a significant advancement in circular bio-economy and sustainability by enabling the efficient, enzyme-driven transformation of bio-based fatty acids into high-value bioplastic precursors. By immobilizing aldehyde reductase on a metal organic framework (MOF) addresses key industrial challenges such as enzyme degradation, high purification costs, and limited recyclability. The enzymatic cascade efficiently converts ω-hydroxy fatty acids derived from agricultural waste into ω-amino fatty acids, which are crucial for producing sustainable polyamides used in bioplastic production. Importantly, this method upcycles renewable biomass into functional materials, aligning with the UN sustainable development goals SDG12 and SDG13 by reducing carbon emissions and plastic pollution.

Plastic pollution has reached an alarming level, with over 400 million metric tons of petroleum plastic produced globally every year.[1] Bioplastic derivatives offer a sustainable and eco-friendly alternative to petrochemical-based plastics. With the rapid deterioration of fossil resources, rational utilization of abundant renewable biomass is regarded as a viable pathway for the sustainable production of industrially important biochemicals.[2] Free fatty acid-rich feedstock from agricultural biomass sources can be employed as a direct precursor for producing various biopolymer intermediates with a broad range of commercial applications in pharmaceutical, surfactant, cosmetic, adhesive, and other industries.[3] For example, lauric acid (C12), decanoic acid (C10), octanoic acid (C8) and hexanoic acid (C6) account for 50% of low-cost palm kernel oil and coconut oil.[4] Furthermore, ω-amino fatty acids (ω-AFAs) and lactams, present in numerous natural and synthetic bioactive compounds, have also been widely used in polyamide production.[5] With the increasing environmental hazards of chemical synthesis, recent years have evidenced a surge in biomanufacturing of eco-friendly and sustainable bioplastics.[6]

Biocatalytic cascades offer the development of a strategic route to economically sustainable and green manufacturing.[7] Aldehyde reductase (AHR) derived from *Synechocystis* species exhibits good activity toward a broad range of aliphatic and aromatic alcohols.[8] Consequently, AHRs have been successfully employed for the conversion of ω-hydroxy fatty acids (ω-HFAs) into their corresponding ω-oxo-fatty acids (ω-OFAs), which are crucial intermediates in the synthesis of bioplastic precursors from renewable biomass.[9] Previously, Yun's group employed the same enzyme together with ω-TA from *S. pomeroyi* (spTA) for the conversion of ω-HFAs and α,ω-diols to ω-AFAs and α,ω-diamines, respectively.[10] However, free enzymes lose their

[a]*BRIC-National Agri-Food and Biomanufacturing Institute (NABI), Department of Biotechnology (DBT), Government of India, Sector 81 (Knowledge City), S. A. S. Nagar 140306, Punjab, India. E-mail: jayeeta@ciab.res.in; jbhaumi@gmail.com; md.patil@ncl.res.in*

[b]*Indian Institute of Science Education and Research (IISER), Knowledge City, Sector 81, Mohali 140306, Punjab, India*

[c]*Chemical Engineering and Process Development Division, CSIR-National Chemical Laboratory, Dr Homi Bhabha Road, Pune, Maharashtra, 411008, India*

[d]*Academy of Scientific and Innovative Research (AcSIR), Ghaziabad 201002, India*

† Electronic supplementary information (ESI) available: Material and instruments, analysis methods, enzyme expression and purification, synthesis of UIO-66-NH_2, post synthesis modification, immobilization of AHR, activity and specific activity of free AHR and AHR@UIO-66-NH_2, substrate concentration optimization, optimization of enzyme concentration, time course study of free AHR and AHR@UIO-66-NH_2, effect of temperature, pH, storage stability and recyclability, relative activity of spTA, conversion of hydroxy fatty acids into amino fatty acids. See DOI: https://doi.org/10.1039/d5su00311c

catalytic activity over time and cannot be employed for repetitive biocatalytic cycles.[11]

Although the purified form of an enzyme is most desired, its synthetic applicability is often limited by high downstream purification costs and poor long-term storage stability.[11,12] Furthermore, mass-transfer limitations, imposing poor substrate accessibility to the enzyme located within a microbial cell, potentially limit the use of whole-cell biocatalysts.[13]

Immobilization of enzymes onto solid surfaces offers an advantageous approach owing to low downstream requirements, improved stability, and reusability in the subsequent batch or continuous reactions.[14,15] Furthermore, newer immobilization strategies are emerging for *in situ* regeneration of cofactors. For example, Betancor *et al.* co-immobilized glucose-6-phosphate dehydrogenase and nitrobenzene nitroreductase for NADPH recycling and continuous conversion of nitrobenzene into hydroxylaminobenzene.[16]

In recent years, there has been a surge in interest in the utilization of metal organic frameworks (MOFs) for the immobilization of various enzymes.[17,18] Compared with traditional porous materials, MOFs offer excellent advantages, including a large surface area and tunable porosity,[19,20] which increase the loading capacity of enzymes and provide higher availability for substrate–enzyme complexation.[19] Zirconium–based UIO-66-NH_2 has demonstrated stability across a wide range of pH, in water, and in numerous other solvents, which supports its applicability in enzyme immobilization.[21] Post-synthetic modification (PSM) of UIO-66-NH_2 with succinic anhydride (SA) offers additional functionalization by introducing carboxyl groups in place of surface amines.[22]

In the present study, a post-synthesis modification strategy was applied to immobilize AHR on UIO-66-NH_2. As illustrated in Scheme 1a, the surface chemistry of UIO-66-NH_2 was modified using succinic anhydride (SA-UIO-66-NH_2), introducing carboxyl groups to the framework. The operational stability of AHR@UIO-66-NH_2 was then evaluated under varying pH and temperature conditions, along with its reusability, using benzaldehyde as a model substrate. Finally, the optimized AHR@UIO-66-NH_2 system was employed for the bioconversion of ω-hydroxy fatty acids (ω-HFAs) into the corresponding ω-oxo fatty acids (ω-OFAs) and further integrated with spTA for the consequent biotransformation of ω-OFAs into ω-AFAs (Scheme 1b).

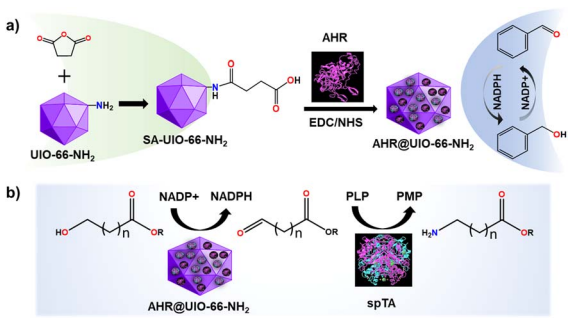

Scheme 1 (a) Immobilization of AHR on UIO-66-NH_2; (b) synthesis of ω-AFAs from their corresponding ω-HFAs.

The study commenced with the transformation of a plasmid harbouring gene of interest into *E. coli BL21* (DE3) competent cells. This step was followed by overexpression and purification of AHR and spTA (see ESI section S2.1, Table S1 and Fig. S1†). Then, purified AHR was used for further investigation. Next, UIO-66-NH_2 was synthesized and characterized using a reported method with slight modification.[21] FTIR analysis confirmed the presence of an –NH stretching peak at 3300, along with C=C and C–O stretching vibrations at 1359 and 1560, respectively. Peaks at 770 and 672 cm^{-1} confirmed the presence of a Zr–O bond (Fig. 1b). Additionally, XRD analysis revealed that the synthesized MOF was crystalline in nature,[23] with characteristic peaks at 2θ = 7.39, 8.60, and 25.81° (Fig. 1c). FESEM micrographs depicted spherical morphology with an average particle size of ~500 nm (Fig. S8†). To gain further insights, HR-TEM analysis was performed, which showed the porous and rough surface morphology of UIO-66-NH_2 (Fig. 1d, S9a and b†). After successful synthesis of MOFs, initial attempts to conjugate AHR directly onto the surface were unsuccessful. Then, we used a post-synthetic modification approach using succinic anhydride to convert amine group on UIO-66-NH_2 into a COOH group, resulting in SA-UIO-66-NH_2. The ratio of succinic anhydride (SA) to UIO-66-NH_2 ranged from 2 : 10 to 12 : 10 (w/w; SA:UIO-66-NH_2), with the optimal conjugation of AHR (>95%) observed at a ratio of 8 : 10 (Table S2†). This was further corroborated by the emergence of a new band at ~1050 cm^{-1} in FTIR analysis after the treatment with SA. Additionally, decrease in the intensity of the band corresponding to amide between 3300 and 3400 cm^{-1} was observed (Fig. 1b).

To validate the immobilization, UV-visible spectra were measured to determine the optical properties of free AHR, UIO-66-NH_2, and AHR@UIO-66-NH_2. The characteristic peak of UIO-66-NH_2 was shifted to around 260 nm after enzyme immobilization (Fig. 1a). In addition, the presence of broad bands at 1050 and 3300–3400 cm^{-1} in FTIR spectra (Fig. 1b) was consistent with previous reports.[19] XRD spectra revealed no changes in the crystallinity of the MOF after PSM (SA-UiO-66-NH_2). However, AHR@UiO-66-NH_2 depicted a decrease in the intensity of the characteristic peaks at 2θ = 7.39 and 8.60, indicating successful immobilization of the enzyme (Fig. 1c). FESEM micrographs showed no change in the morphology of UIO-66-NH_2 post immobilization. (Fig. S8†). In contrast, high resolution TEM images revealed a smooth surface for AHR@UIO-66-NH_2, suggesting the formation of an enzyme layer on the MOF surface (Fig. 1e, S9c and d†), whereas the bare MOF exhibited a rough surface. Furthermore, line profiling of UIO-66-NH_2 showed distinct and regularly spaced peaks, indicative of well-ordered and uniform pore structures (Fig. 1f). In contrast, the line profile of AHR@UIO-66-NH_2 displayed broader and less defined peaks, suggesting a more disordered or partially amorphous structure (Fig. 1g). These observations from HRTEM imaging and line profiling indicate that enzyme immobilization altered the surface morphology of UIO-66-NH_2, changing it from a rough and porous texture to a smoother and less ordered structure. From these results, it can be inferred that AHR was successfully immobilized onto the modified UIO-66-NH_2. Furthermore, buffer analysis revealed >90% of enzyme

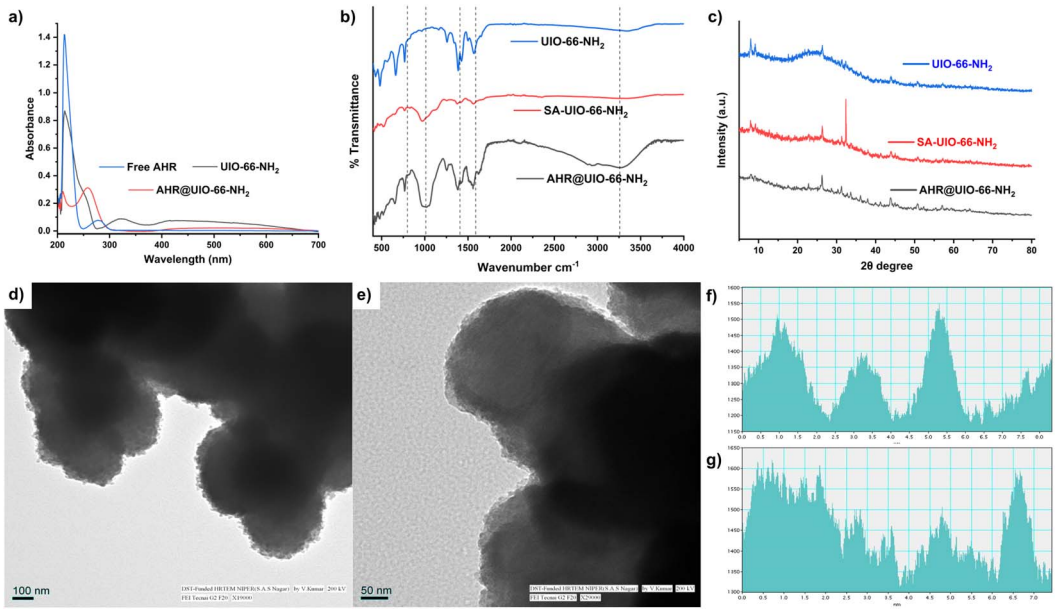

Fig. 1 (a) UV-Visible spectra of UIO-66-NH_2, free AHR, and AHR-UIO-66-NH_2; (b) FTIR spectra of Free AHR, UIO-66-NH_2, SA-UIO-66-NH_2, and AHR-UIO-66-NH_2; (c) XRD spectra of UIO-66-NH_2, SA-UIO-66-NH_2, and AHR-UIO-66-NH_2; (d) HRTEM image of UIO-66-NH_2 (scale 100 nm); (e) HRTEM image of AHR@UIO-66-NH_2 (scale 50 nm); (f) line profiling of UIO-66-NH_2l and (g) line profiling of AHR@UIO-66-NH_2.

immobilization using sodium phosphate and Tris buffer, whereas other buffers showed <50% of immobilization (Table S3†).

Later, the optimal immobilization capacity of UIO-66-NH_2 was determined by varying the enzyme to MOF ratio (w/w) from 0.4 : 10 to 2.5 : 10. At a ratio of 0.95 : 10, an enzyme loading of >95% was achieved, while retaining ~90% enzyme activity (Table S4†). Beyond the optimal loading capacity, a decline in enzyme activity suggested that maximal immobilization capacity was achieved. Therefore, this modified UIO-66-NH_2 demonstrated good immobilization capacity (95 mg g^{-1}) compared with MOFs reported in previously published studies (Table S10†).

Subsequently, enzyme activities of free AHR and AHR@UIO-66-NH_2 were tested against benzaldehyde as a model substrate (Fig. S2†). Notably, all the conversions were analyzed using gas chromatography–mass spectroscopy (GC-MS). The free enzyme achieved 94% conversion of benzaldehyde into benzyl alcohol, while the immobilized enzyme reached 84% conversion (Table S5†). Furthermore, the specific activity of free AHR and AHR@UIO-66-NH_2 calculated for the benzaldehyde substrate was 0.0075 and 0.0045 μM min^{-1} μg^{-1}, respectively (Table S6†). The decreased specific activity of AHR@UIO-66-NH_2 might be explained by mass transfer limitation or loss of the integrity of the active site after immobilization.[24]

Later, benzaldehyde concentration for the enzyme-catalyzed reaction was optimized using different concentrations from 10 to 80 mM while keeping other parameters unaltered. For a benzaldehyde concentration of up to 30 mM, >95% conversion was observed. In contrast, the conversion reduced to 20% at benzaldehyde concentrations above 30 mM, possibly owing to substrate toxicity towards enzyme (Fig. S3†). Notably, cofactor concentration was kept constant across all the reactions. No noticeable change in the reaction was observed when AHR/AHR@UIO-66-NH_2 was used in the range of 20–300 μg (Fig. S4†). Time course data revealed that free AHR efficiently achieved >85% conversion, whereas AHR@UIO-66-NH_2 achieved <65% conversion in 60 min (Fig. S5†). To check the buffer compatibility of the prepared biocatalysts, the activity of free AHR and AHR@UIO-66-NH_2 was analyzed in different buffers. Free AHR demonstrated >90% conversion of benzaldehyde in Tris and HEPES buffers, whereas the conversion achieved by AHR@UIO-66-NH_2 was >85% in Tris, sodium phosphate and MES buffers (Table S7†). Thermal stability studies further

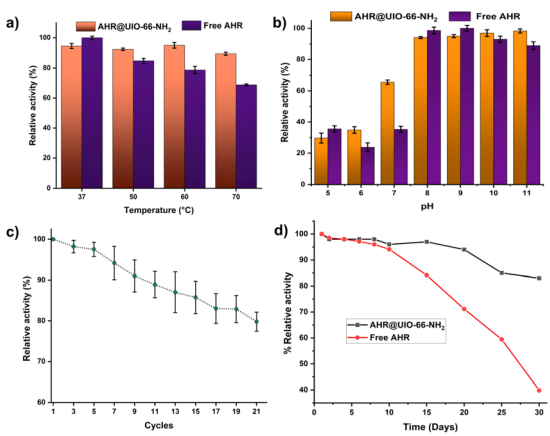

Fig. 2 (a) Temperature sensitivity of AHR@UIO-66-NH_2 and free AHR, (b) pH tolerance of free and UIO-66-NH_2, (c) recyclability of immobilized enzyme, (d) storage stability of immobilized enzyme in Tris buffer.

revealed that at 60 °C, AHR@UIO-66-NH_2 retained 93% of its activity, compared with 77% for free AHR (Fig. 2a). While increasing the temperature to 70 °C led to a decline in the activity of free AHR, the immobilized enzyme maintained 87% of its activity. The improved thermal stability of the enzyme was possibly due to the formation of a stable noncovalent bond between the enzyme and the MOF material, which enhanced the rigidity of the protein's secondary structure, protecting the active conformation from destruction.[25]

The pH value of the catalytic environment had a significant effect on the enzyme-catalyzed reactions. The impact of pH on enzyme activity was evaluated in the pH range of 5.0–11. The relative activity of free AHR was low under acidic conditions and high under alkaline conditions. However, AHR@UIO-66-NH_2 showed twofold higher activity at neutral pH compared with free AHR (Fig. 2b). These results reveal that the combination of the enzyme and the carrier created a protected microenvironment that led to an increase in optimum pH.[26]

Finally, to check the stability of the immobilized enzyme over the free counterpart, free AHR and AHR@UIO-66-NH_2 were incubated at 4 °C for 30 days in tris buffer. Notably, free AHR retained only 40% of its initial catalytic activity, whereas AHR@UIO-66-NH_2 retained more than 80% of its initial catalytic efficiency (Fig. 2c). This finding suggests that the stability of immobilized AHR@UIO-66-NH_2 was significantly enhanced compared with that of the free enzyme. The recyclability of AHR@UIO-66-NH_2 was tremendously increased compared with that of free AHR. Even after 21 consecutive cycles of use, the immobilized enzyme retained approximately 80% of its initial catalytic activity (Fig. 2d), indicating that UIO-66-NH_2 provides effective stabilization and minimizes enzyme loss during repeated use. The stability and robustness of immobilized enzymes underscore their potential for application in continuous production processes within the bioplastic industry.

Finally, to validate the efficacy of the prepared biocatalyst, a biocatalytic cascade was established for the synthesis of ω-AFAs from their corresponding ω-HFAs). This cascade involved AHR@UIO-66-NH_2 in combination with the optimized ω-transaminase from *S. pomeroyi* (spTA) (see ESI Section S4, Fig. S6 and Table S8†). As model substrates, 8-hydroxy octanoic acid (8 HOA), 10-hydroxy decanoic acid (10 HDA), and 12-hydroxy dodecanoic acid (12 HDDA) were selected. Following a previously reported protocol,[9] 20 mM of ω-HFAs was used as a substrate, with benzylamine serving as the amine donor. $NADP^+$ and PLP were used as cofactors for AHR/AHR@UIO-66-NH_2 and spTA, respectively. When free AHR and the spTA system were employed in the cascade, >90% conversion of 8 HOA, 10 HDA, and 12 HDDA to their corresponding amino fatty acids was observed. Subsequently, the tandem system comprising AHR@UIO-66-NH_2 and spTA was applied to the same substrates under similar conditions, which resulted in 85%, 80%, and 71% conversions for 8 HOA, 10 HDA, and 12 HDDA, respectively (Fig. 3 and Table S9†). These comparable conversions highlight the potential of the immobilized system for industrial applications in the sustainable synthesis of ω-amino fatty acids.

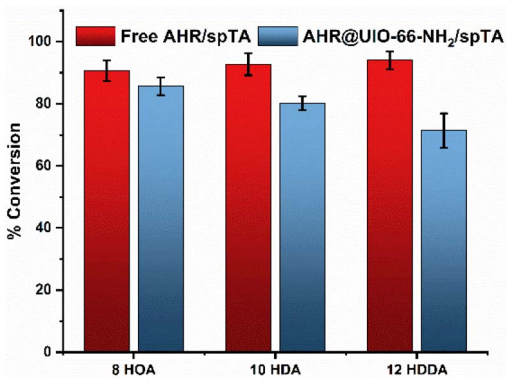

Fig. 3 Conversion of ω-HFAs into corresponding ω-AFAs using free AHR/spTA and the AHR@UIO-66-NH_2/spTA system.

Conclusion

In summary, we present a sustainable strategy for efficiently converting bio-based fatty acids into bioplastic precursors using enzyme immobilization. AHR was covalently anchored onto MOF UIO-66-NH_2 *via* EDC-NHS coupling. The specific activity of AHR and AHR@UIO-66-NH_2 against benzaldehyde was found to be 0.0075 and 0.0045 μM min^{-1} μg^{-1}, respectively. Notably, AHR@UIO-66-NH_2 retained 80% of its activity even after 30 days and demonstrated robust reusability over 21 cycles. The immobilized enzyme enabled a cascade transformation of 8-, 10-, and 12-hydroxy fatty acids into amino fatty acids as key bioplastic precursors. This sustainable approach for valorizing and upscaling biomass-based fatty acids into bioplastic precursors (as an alternative to petroleum-based plastic) directly contributes to biomanufacturing.

Data availability

The data supporting this article have been included as part of the ESI.†

Conflicts of interest

There are no conflicts to declare.

Acknowledgements

The authors thank Department of Biotechnology (DBT), Govt. of India, for funding M. D. P through M. K. Bhan Young Researcher fellowship. J. B., Y. N. R., and D. M. thank DBT for funding under the lignin valorization project. K. R. is grateful to the UGC for providing a fellowship. Both D. M. and K. R. are registered for Ph.D. at IISER Mohali. The authors gratefully acknowledge Prof. Hyungdon Yun, Konkuk University, Seoul, South Korea, for providing the plasmids harboring the genes studied herein.

Notes and references

1 N. Singh and T. R. Walker, *npj Mater. Sustain.*, 2024, **2**, 17.
2 H. Kawaguchi, C. Ogino and A. Kondo, *Bioresour. Technol.*, 2017, **245**, 1664–1673.
3 H. Kim, S. Lee, Y. Ahn, J. Lee and W. Won, *ACS Sustain. Chem. Eng.*, 2020, **8**, 12419–12429.
4 P. G. Roopashree, S. S. Shetty and N. Suchetha Kumari, *J. Funct. Foods*, 2021, **87**, 104724.
5 Y. Zhou, R. Lu, X. Gao, L. Lin, Y. Wei and X.-J. Ji, *RSC Sustainability*, 2025, **3**, 2149–2159.
6 A. Krishnamurthy and P. Amritkumar, *SN Appl. Sci.*, 2019, **1**, 1432.
7 L. Lin, R. Ledesma-Amaro, X.-J. Ji and H. Huang, *Trends Biotechnol.*, 2023, **41**, 150–153.
8 M. K. Akhtar, N. J. Turner and P. R. Jones, *Proc. Natl. Acad. Sci. U. S. A.*, 2013, **110**, 87–92.
9 H.-W. Yoo, H. Jung, S. Sarak, Y. C. Kim, B. G. Park, B.-G. Kim, M. D. Patil and H. Yun, *Green Chem.*, 2022, **24**, 2222–2231.
10 S. Sung, H. Jeon, S. Sarak, M. M. Ahsan, M. D. Patil, W. Kroutil, B. G. Kim and H. Yun, *Green Chem.*, 2018, **20**, 4591–4595.
11 B. P. Dwivedee, J. Bhaumik, S. K. Rai, J. K. Laha and U. C. Banerjee, *Bioresour. Technol.*, 2017, **239**, 464–471.
12 F. Lyu, Y. Zhang, R. N. Zare, J. Ge and Z. Liu, *Nano Lett.*, 2014, **14**, 5761–5765.
13 M. D. Patil, G. Grogan, A. Bommarius and H. Yun, *Catalysts*, 2018, **8**, 254.
14 S. K. Rai, H. Kaur, B. S. Kauldhar and S. K. Yadav, *ACS Biomater. Sci. Eng.*, 2020, **6**, 6661–6670.
15 M. Ashjari, M. Garmroodi, F. Ahrari, M. Yousefi and M. Mohammadi, *Chem. Commun.*, 2020, **56**, 9683–9686.
16 L. Betancor, C. Berne, H. R. Luckarift and J. C. Spain, *Chem. Commun.*, 2006, **34**, 3640–3642.
17 Q. Chen, C. Wu, S. Hu, L. Cui, Y. Zhang, P. Hu, Z. Xu, P. Yu and M. Yu, *New J. Chem.*, 2024, **48**, 17246–17253.
18 Y. N. Reddy, A. De, S. Paul, A. K. Pujari and J. Bhaumik, *Biomacromolecules*, 2023, **24**, 1717–1730.
19 X. Yuan, Y. Liu, F. Cao, P. Zhang, J. Ou and K. Tang, *AIChE J.*, 2020, **66**, e16292.
20 Y. Ma, C. Sun, Q. Zhang, Y. Ren, Q. Zeng, F. Cao, B. Sun, P. Zhang and K. Tang, *Mol. Catal.*, 2023, **553**, 113750.
21 M. A. Bunge, A. B. Davis, K. N. West, C. W. West and T. G. Glover, *Ind. Eng. Chem. Res.*, 2018, **57**, 9151–9161.
22 A. Enríquez-Cabrera, K. Ridier, L. Salmon, L. Routaboul and A. Bousseksou, *Eur. J. Inorg. Chem.*, 2021, **2021**, 2000–2016.
23 C. S. Hinde, W. R. Webb, B. K. J. Chew, H. R. Tan, W.-H. Zhang, T. S. A. Hor and R. Raja, *Chem. Commun.*, 2016, **52**, 6557–6560.
24 Y. Wu, W. Xu, L. Jiao, W. Gu, D. Du, L. Hu, Y. Lin and C. Zhu, *Chem. Soc. Rev.*, 2022, **51**, 6948–6964.
25 Q. Chen, C. Wu, S. Hu, L. Cui, Y. Zhang, P. Hu, P. Yu, Z. Xu and M. Yu, *New J. Chem.*, 2024, **48**, 17246–17253.
26 X. Liu, Y. Hu, B. Wei, F. Liu, H. Xu, C. Liu, Y. Li and H. Liang, *Process Biochem.*, 2022, **118**, 323–334.